Deep-Sea Research I 58 (2011) 668–676

Contents lists available at ScienceDirect

Deep-Sea Research I

journal homepage: www.elsevier.com/locate/dsri

# An approximate solution of wave-modified Ekman current for gradually varying eddy viscosity☆

Jin-Bao Song [a,b,*], Yan-Song Huang [a,b,c]

[a] Institute of Oceanology, Chinese Academy of Sciences, Nanhai road 7, Qingdao 266071, PR China
[b] Key Laboratory of Ocean Circulation and Waves (KLOCAW), Chinese Academy of Sciences, Qingdao 266071, PR China
[c] Graduate University of Chinese Academy of Sciences, Beijing 100039, PR China

ARTICLE INFO

*Article history:*
Received 26 August 2010
Received in revised form
3 April 2011
Accepted 7 April 2011
Available online 14 April 2011

*Keywords:*
Ekman current
Random wave
Stokes drift
Eddy viscosity coefficient

ABSTRACT

An approximate steady solution of the wave-modified Ekman current is presented for gradually varying eddy viscosity by using the WKB method with the variation of parameters technique. The parameters involved in the solution can be determined by the two-dimensional wavenumber spectrum of ocean waves, wind speed, the Coriolis parameter and the densities of air and water. The solution reduces to the exact solution when the eddy viscosity is taken as a constant. As illustrative examples, for a fully developed wind-generated sea with different wind speeds and a few proposed gradually varying eddy viscosities, the current profiles calculated from the approximate solutions are compared with those of the exact solutions or numerical ones by using the Donelan and Pierson wavenumber spectrum, the WAM wave model formulation for wind input energy to waves, and wave energy dissipation converted to currents. It is shown that the approximate solution presented has an elegant form and yet would be valid for any given gradually varying eddy viscosity. The applicability of the solution method to the real ocean is discussed following the comparisons with published observational data and with the results from a large eddy simulation of the Ekman layer.



## 1. Introduction

The effects of wind-driven surface gravity waves on ocean surface currents have been recognized to play a crucial role for scientific and engineering applications. For example, they are important in the interpretation of satellite images and the impact of surface currents on satellite-derived wind estimates (Quilfen et al., 2001; Kelly et al., 2001), the correction of biases in radar-derived surface currents (Chapron et al., 2005), sea ice drift (Tang and Gui, 1996), various biological processes such as the drift of fish eggs and larvae (Brickman and Frank, 2000; Reiss et al., 2000), environmental loading on offshore structures (Farmer et al., 1995), the dispersion and drift of oil and other pollutants (Leibovich, 1997a, 1997b; Morinta et al., 1997), hurricane intensities (Emanuel, 1999; Andreas and Emanuel, 2001) and climate (Tang et al., 2002).

Waves grow and evolve in space and time, interacting with ocean currents and reflecting the structure and development of the wind stress fields that generate them. As they experience wave breaking and dissipation, momentum passes from waves into ocean currents. Using irrotational theory for wave growth and wave breaking, Weber (1983), Weber and Melsom (1993) and Melsom (1996) investigated the conversion of the wave pseudo-momentum to momentum of the mean Eulerian current from wave dissipation caused by the eddy viscosity. Jenkins (1986, 1987a, 1987b, 1989) developed the corresponding formulation based on an ocean spectral wave model. Perrie et al. (2003) and Tang et al. (2007) coupled the formulation of Jenkins (1987a, 1987b, 1989) to an ocean model to investigate the impact of waves on surface currents. They showed that the wave effect could increase the surface current by as much as 40%.

Recent studies show that the influence of the surface wave motion via the Stokes drift and mixing is fundamental to understanding the observed Ekman current profiles (Lewis and Belcher, 2004; Polton et al., 2005; Rascle et al., 2006), although real Ekman currents are the products of a host of interrelated factors, including wind stress, surface wave motion, surface heating and so on. Following the approach of Jenkins (1987a, 1987b, 1989) and Perrie et al. (2003), Song (2009) presented the steady analytic solutions for modified Ekman equations including random surface wave effects when the eddy viscosity coefficient is, respectively,

☆The research presented in this paper was supported by the National Natural Science Foundation of China (no. 40876012), the National Basic Research Program of China (no. 2011CB403501) and the Fund for Creative Research Groups by NSFC (no. 40821004).

* Corresponding author at: Institute of Oceanology, Chinese Academy of Sciences, Nanhai road 7, Qingdao 266071, PR China. Tel./fax: +86 532 82898506.
*E-mail address:* songjb@qdio.ac.cn (J.-B. Song).

0967-0637/$ - see front matter © 2011 Elsevier Ltd. All rights reserved.
doi:10.1016/j.dsr.2011.04.001

taken as depth-independent and proportional to depth. The effects of random waves on the classical Ekman current are then studied by comparing the solutions including waves to those with no waves. In this paper, an approximate solution of the model used by Song (2009) is presented for gradually varying eddy viscosities using the WKB method, and this WKB solution is studied and compared with the exact and numerical solutions of the model for a few proposed eddy viscosities. Possible applications of the solution method to the real ocean are discussed.

## 2. Basic equations and boundary conditions

When the effects of random surface waves are considered, the steady wind-driven Ekman horizontal current satisfy the following modified Ekman equation (Jenkins, 1989; Rascle et al., 2006; Tang et al., 2007; Song, 2009)

$$A_v(z)\frac{\partial^2 U_{WE}(z)}{\partial^2 z}+\frac{\partial A_v(z)}{\partial z}\left[\frac{\partial U_{WE}(z)}{\partial z}\right]-ifU_{WE}(z)=ifU_s(z)+T_{wds}(z), \tag{1}$$

where $U_{WE}=u_{WE}+iv_{WE}$ is the complex horizontal velocity in the $x$–$y$ plane, $i=\sqrt{-1}$, $f$ is the Coriolis parameter. The horizontal coordinate axes are fixed on the still water level with $z=0$, the $z$-axis is along the vertical direction with positive direction upwards, $A_v(z)$ is the vertical eddy viscosity coefficient, $U_s=u_s+iv_s$ is the complex Stokes drift, and $T_{wds}$ is the wave-induced momentum transfer from waves to the mean flow due to dissipation of wave energy. The velocity $\mathbf{u}_{WE}=(u_{WE},v_{WE})$ discussed here is the quasi-Eulerian current, which is equal to the Lagrangian mean current minus the Stokes drift and can be understood as the Eulerian-mean current as stated by Jenkins (1987a; 1989) and Perrie et al. (2003).

The surface boundary condition for the modified Ekman current is

$$A_v\frac{\partial U_{WE}}{\partial z}=\frac{\tau_a}{\rho_w}-\frac{\tau_{in}}{\rho_w},\quad z=0, \tag{2}$$

where $\rho_w$ is the water density, $\tau_{in}$ is the reduction of wind stress due to wave generations, $\tau_a=\tau_{ax}+i\tau_{ay}$ is the complex wind stress, computed from surface wind field $\mathbf{U}_{10}$ at 10 m height,

$$\boldsymbol{\tau}_a=(\tau_x,\tau_y)=\rho_a C_d|U_{10}|\mathbf{U}_{10}, \tag{3}$$

$\rho_a$ is the air density, and $C_d$ is the air-sea drag coefficient, which is related to $U_{10}$ by the following relation (Wu, 1982):

$$C_d=(0.8+0.065U_{10})\times 10^{-3}. \tag{4}$$

The lower boundary condition is taken as

$$U_{WE}\to 0,\quad (z\to-\infty). \tag{5}$$

$\tau_{in}$ and $T_{wds}$ can be estimated by the source terms from a directional spectral wave prediction model that act to transfer momentum from the wave field to the current as follows (Jenkins, 1989, also see Tang et al., 2007):

$$\tau_{in}=\tau_{inx}+i\tau_{iny}=\rho_w\int\left(\frac{\omega}{k}\right)KS_{in}(k,\theta)dk\,d\theta, \tag{6}$$

$$T_{wds}=T_{wdsx}+iT_{wdsy}=2\int\omega Ke^{2kz}S_{ds}(k,\theta)dk\,d\theta, \tag{7}$$

where $\omega$ is the angular frequency in rad/s, $k$ is the moduli of the horizontal wavenumber vector $\mathbf{k}=(k_x,k_y)=(k\cos\theta,k\sin\theta)$, their relationship is given by the dispersion relation $\omega^2=gk$, $\theta$ is the angle between the wave vector and the $x$-axis, $K=k_x+ik_y$, $S_{in}(k,\theta)$ is the wind input energy to waves, $S_{ds}(k,\theta)$ is the wave energy lost by wave dissipation mechanisms as represented in third-generation WAM-type models (Hasselmann et al., 1988; Komen et al., 1994).

Stokes drift $\mathbf{u}_s$ may be expressed as (Kenyon, 1969; Huang, 1971)

$$\mathbf{u}_s=2\int\omega\mathbf{k}e^{2kz}E(k,\theta)dk\,d\theta, \tag{8}$$

where $E(k,\theta)$ is the directional wavenumber spectrum of surface waves.

## 3. Approximate solutions

Eq. (1) is a linear inhomogeneous ordinary differential equation with variable coefficients if the eddy viscosity $A_v(z)$ is specified. Thus, it can then be solved by ordinary differential equation methods. Following Berger and Grisogono (1998), studying the Ekman atmospheric boundary layer, an approximate solution to the inhomogeneous problem (1) can be found with the variation of parameters technique, provided that an approximate solution to the homogeneous problem of (1) exists. If two independent approximate solutions to homogeneous problem of Eq. (1) are given by $\Phi_1(z)$ and $\Phi_2(z)$, the general solution of Eq. (1) is given by

$$U_{WE}(z)=[\hat{c}_1\Phi_1(z)+\hat{c}_2\Phi_2(z)]+[c_1(z)\Phi_1(z)+c_2(z)\Phi_2(z)], \tag{9}$$

where $\hat{c}_1$ and $\hat{c}_2$ are constants, $\hat{c}_1\Phi_1(z)+\hat{c}_2\Phi_2(z)$ represents the complementary solution, and $c_1(z)\Phi_1(z)+c_2(z)\Phi_2(z)$ is the particular solution with

$$c_1(z)=-\int_0^z\frac{\Phi_2(z')\eta(z')}{F(z')}dz', \tag{10}$$

$$c_2(z)=\int_0^z\frac{\Phi_1(z')\eta(z')}{F(z')}dz', \tag{11}$$

where

$$F(z')=A_v(z')\left[\Phi_1(z')\Phi_2'(z')-\Phi_1'(z')\Phi_2(z')\right], \tag{12}$$

and $\eta(z')=ifU_s(z')+T_{wds}(z')$ is the inhomogeneous part of Eq. (1).

To find the homogeneous solutions $\Phi_1(z)$ and $\Phi_2(z)$, following Grisogono (1995) in a study of the atmospheric Ekman layer, the WKB method is applied. The first and third terms in the left of Eq. (1) represent the control behavior, which is the basis of the WKB analysis, while the second term is identified with the modifications due to departures of $A_v$ from constant. The WKB expansion for $U_{WE}$ can be expressed in the form

$$U_{WE}\propto\exp\{(S_0+S_1\varepsilon+S_2\varepsilon^2+\cdots)/\varepsilon\}. \tag{13}$$

The WKB approach can provide a good approximate solution, so long as the properties of the medium vary at least slightly slower than the calculated quantities.

Substituting Eq. (13) into Eq. (l), we obtain a set of equations in terms of powers of a presumably small parameter $\varepsilon$ ($\varepsilon$ has been introduced on account of the above-mentioned balance between the terms and at a later stage it will be equated to unity).

As analyzed by Grisogono (1995), the validity of the WKB method requires that the variable eddy viscosity does not vary too quickly with depth, $A_v$ and $f$ do not change their signs and that:

$$\frac{|S_{n+1}(z)|}{|S_n(z)|}<<1,\quad n=0,\ 1,\ 2,\ldots, \tag{14}$$

over the intervals. Also, if $S_N$ is the last term used in the series,

$$|S_{N+1}(z)|<<1. \tag{15}$$

The first two terms of the expansion are sufficient to give a meaningful, yet simple solution. Solving for $S_0$ and $S_1$ yields

$$S_0=\pm(1+i)\sqrt{\frac{f}{2}}\int_0^z\frac{1}{\sqrt{A_v(z')}}dz', \tag{16}$$

and

$$S_1 = \frac{1}{4}\ln\left(\frac{A_v(0)}{A_v(z)}\right). \tag{17}$$

So we have two approximate homogeneous solutions of Eq. (1)

$$\Phi_1(z) = B(z)\exp(D(z)), \tag{18}$$

$$\Phi_2(z) = B(z)\exp(-D(z)), \tag{19}$$

where

$$B(z) = \left(\frac{A_v(0)}{A_v(z)}\right)^{1/4}, \quad D(z) = (1+i)\sqrt{\frac{f}{2}}\int_0^z \frac{1}{\sqrt{A_v(z')}}dz'. \tag{20}$$

The functions $c_1(z)$ and $c_2(z)$ can be expressed as

$$c_1(z) = \frac{1-i}{2\sqrt{2fA_v(0)}}\int_0^z B(z')[ifU_s(z')+T_{wds}(z')]\exp(-D(z'))dz', \tag{21}$$

$$c_2(z) = -\frac{1-i}{2\sqrt{2fA_v(0)}}\int_0^z B(z')[ifU_s(z')+T_{wds}(z')]\exp(D(z'))dz'. \tag{22}$$

Using the boundary conditions (2), (5), and Eqs. (18)–(22), the constant $\hat{c}_1$ and $\hat{c}_2$ in Eq. (9) can be determined as follows:

$$\hat{c}_1 = \frac{\Phi_0\Phi_2(-\infty)-\Phi_2'(0)\Phi_\infty}{\Phi_1'(0)\Phi_2(-\infty)-\Phi_2'(0)\Phi_1(-\infty)}, \tag{23}$$

$$\hat{c}_2 = \frac{\Phi_\infty\Phi_1'(0)-\Phi_0\Phi_1(-\infty)}{\Phi_1'(0)\Phi_2(-\infty)-\Phi_2'(0)\Phi_1(-\infty)}, \tag{24}$$

where

$$\Phi_0 = \frac{\tau_a-\tau_{in}}{A_v(0)\rho_w}, \tag{25}$$

$$\Phi_\infty = -c_1(-\infty)\Phi_1(-\infty)-c_2(-\infty)\Phi_2(-\infty), \tag{26}$$

and primes denote $z$-derivatives.

## 4. Solution for a kind of depth-dependent eddy viscosity

As noted by Jenkins (1989), the Ekman surface current is directed at 45° to the right of the wind direction in the northern hemisphere if the eddy viscosity is assumed to be constant, which is inconsistent with the field observations of surface drift current, reviewed by Huang (1979). In fact, there are several approaches to estimate the vertical eddy viscosity $A_v$. Many measurements have been made to determine its value, and different parameterizations have been proposed. A collection of values and functional forms can be found in Huang (1979) and Santiago-Mandujano and Firing (1990).

Although atmospheric turbulent boundary layers basically obey logarithmic velocity profiles, corresponding to a linear increase in eddy viscosity with height, it is very difficult to establish the presence of a log profile in a turbulent oceanic boundary layer because of surface waves and wave breaking. McWilliams et al. (1997) and Zikanov et al. (2003) computed the eddy viscosity by using large eddy simulations of the ocean mixed layer, and demonstrated that it follows a convex shape. Madsen (1977) examined the problem by assuming that the eddy viscosity increases linearly with depth throughout the mixed layer. Witten and Thomas (1976) used a vertical eddy viscosity that decreases exponentially with depth in the study of wind-driven currents in shallow water. In this paper, we assume that the eddy viscosity can be expressed as follows:

$$A_v(z) = A_v(0)(1-\delta z)\exp(\alpha z), \tag{27}$$

where, $A_v(0)$ is the surface eddy viscosity, $\delta$ and $\alpha$ are positive constants. It is noted that this kind of the eddy viscosity (27) is the generalization of many previously used ones stated as follows:

Substituting this form (27) into Eqs. (18)–(20), (23) and (24), we have

$$B(z) = (1-\delta z)^{-1/4}\exp\left(-\frac{\alpha}{4}z\right), \tag{28}$$

$$D(z) = (1+i)\sqrt{\frac{f}{2A_v(0)}}\int_0^z (1-\delta z')^{-1/2}\exp\left(-\frac{\alpha}{2}z'\right)dz', \tag{29}$$

$$\Phi_1(-\infty) = 0, \quad \Phi_1'(0) = \frac{1}{4}(\delta-\alpha)+(1+i)\sqrt{\frac{f}{2A_v(0)}}, \tag{30}$$

$$\Phi_2'(0) = \frac{1}{4}(\delta-\alpha)-(1+i)\sqrt{\frac{f}{2A_v(0)}}, \tag{31}$$

$$\hat{c}_1 = \frac{\Phi_0+\Phi_2'(0)c_2(-\infty)}{\Phi_1'(0)}, \quad \hat{c}_2 = -c_2(-\infty), \tag{32}$$

and the WKB approximate solution can be calculated by Eqs. (9), (18), (19), (21), (22) and (28)–(32).

### 4.1. Case 1, eddy viscosity is independent of water depth

If $A_v$ is depth-independent, which corresponds to the case of $\delta=\alpha=0$ in Eq. (27), we have

$$B(z) = 1, \quad D(z) = (1+i)\sqrt{\frac{f}{2A_v}}z \equiv jz, \tag{33}$$

$$\Phi_1(z) = e^{jz}, \quad \Phi_2(z) = e^{-jz}, \tag{34}$$

$$c_1(z) = \frac{1}{2jA_v}\int_0^z \left[ifU_s(z')+T_{wds}(z')\right]e^{-jz'}dz', \tag{35}$$

$$c_2(z) = -\frac{1}{2jA_v}\int_0^z \left[ifU_s(z')+T_{wds}(z')\right]e^{jz'}dz', \tag{36}$$

$$\hat{c}_1 = \frac{\tau_a-\tau_{in}}{A_v j\rho_w} - \frac{1}{2jA_v}\int_{-\infty}^0 \left[ifU_s(z')+T_{wds}(z')\right]e^{jz'}dz', \tag{37}$$

$$\hat{c}_2 = -\frac{1}{2jA_v}\int_{-\infty}^0 \left[ifU_s(z')+T_{wds}(z')\right]e^{jz'}dz', \tag{38}$$

and the solution (9) reduces to

$$U_{WE1}(z) = \left[\frac{\tau_a-\tau_{in}}{A_v j\rho_w} - \frac{1}{jA_v}\int_{-\infty}^0 [ifU_s(z')+T_{wds}(z')]\cosh(jz')dz'\right]e^{jz} + \frac{1}{jA_v}\int_{-\infty}^z [ifU_s(z')+T_{wds}(z')]\sinh[j(z-z')]dz'. \tag{39}$$

It is noted that the solution (39) is exactly the same as the analytical solution presented by Song (2009). Thus, the approximate solution obtained here includes the exact solution for depth-independent eddy viscosity as a special example.

### 4.2. Case 2, eddy viscosity increasing linearly with depth

Taking $\alpha=0$ in Eq. (27), we have

$$A_v = A_v(0)(1+\delta z_+), \tag{40}$$

where $z_+=-z>0$. The exact solution of Eqs. (1)–(5) for the eddy viscosity (40) is presented by (A.6) in Appendix A. If we take $A_v(0)=\kappa u_* z_{0S}$ and $\delta=1/z_{0S}$ with $z_{0S}$ as the sea surface roughness length scale, $\kappa=0.4$ is von Karmen's constant, and $u_*=(|\boldsymbol{\tau}_a|/\rho_w)^{1/2}$ is the oceanic friction velocity associated with the magnitude of the surface stress, then the eddy viscosity relation (40) is the same as that used by Lewis and Belcher (2004) and Song (2009).

Substituting this form (40) of $A_v$ into Eqs. (18)–(26), we have

$$B(-z_+) = (1+\delta z_+)^{-1/4}, \quad D(-z_+) = (1+i)\sqrt{\frac{2f}{A_v(0)}}\frac{1}{\delta}\left(1-\sqrt{1+\delta z_+}\right), \tag{41}$$

$$\Phi_1(z) \equiv \Phi_1(-z_+) = B(-z_+)e^{D(-z_+)}, \quad \Phi_2(z) \equiv \Phi_2(-z_+) = B(-z_+)e^{-D(-z_+)}, \tag{42}$$

$$c_1(z) = -\frac{1-i}{2\sqrt{2fA_v(0)}}\int_0^{z_+} B(-z'_+)[ifU_s(-z'_+)+T_{wds}(-z'_+)]e^{-D(-z'_+)}dz'_+, \tag{43}$$

$$c_2(z) = \frac{1-i}{2\sqrt{2fA_v(0)}}\int_0^{z_+} B(-z'_+)[ifU_s(-z'_+)+T_{wds}(-z'_+)]e^{D(-z'_+)}dz'_+, \tag{44}$$

$$\hat{c}_1 = \left\{\frac{\tau_a-\tau_{in}}{A_v(0)\rho_w} - \hat{c}_2\left[\frac{\delta}{4}-(1+i)\sqrt{\frac{f}{2A_v(0)}}\right]\right\}\left[\frac{\delta}{4}+(1+i)\sqrt{\frac{f}{2A_v(0)}}\right]^{-1}, \tag{45}$$

$$\hat{c}_2 = -\frac{1-i}{2\sqrt{2fA_v(0)}}\int_0^{+\infty} B(-z'_+)[ifU_s(-z'_+)+T_{wds}(-z'_+)]e^{D(-z'_+)}dz'_+, \tag{46}$$

The solution of Eq. (9) reduces to

$$U_{WE2} = -\frac{(1-i)B(-z_+)}{\sqrt{2fA_v}(0)}\int_0^{z_+} B(-z'_+)[ifU_s(-z'_+)+T_{wds}(-z'_+)] \times \sinh[D(-z_+)-D(-z'_+)]dz'_+ + \hat{c}_1 B(-z_+)e^{D(-z_+)} + \hat{c}_2 B(-z_+)e^{-D(-z_+)}. \tag{47}$$

To compare the approximation solution (47) with the corresponding exact solution (A.6), we calculated the solution by taking $\rho_a = 1.2\ \mathrm{kg\,m^{-3}}$, $\rho_w = 1025\ \mathrm{kg\,m^{-3}}$, $f = 10^{-4}\,\mathrm{s^{-1}}$ for a fully developed wind-generated sea described by the wavenumber spectrum of Donelan and Pierson (1987),

$$E(k,\theta) = \frac{0.00162\times U_{10}}{k^{2.5}g^{0.5}}\exp\left(-\frac{g^2}{k^2(1.2U_{10})^4}\right)1.7^{\Gamma} \times \mu\left(\frac{k}{k_p}\right)\mathrm{sech}^2\left[\mu\left(\frac{k}{k_p}\right)\theta\right](0<k<\infty, -\pi<\theta<\pi), \tag{48}$$

where $\theta$ is the wave direction relative to the wind (the direction of wind is assumed to be along the $x$-axis) and

$$\Gamma = \exp\left\{-1.22\left[\frac{1.2U_{10}k^{0.5}}{g^{0.5}}-1\right]^2\right\}, \tag{49}$$

$$\mu\left(\frac{k}{k_p}\right) = \begin{cases} 1.24 & 0<k/k_p<0.31 \\ 2.61(k/k_p)^{0.65} & 0.31<k/k_p<0.9 \\ 2.28(k_p/k)^{0.65} & 0.9<k/k_p<10 \end{cases}. \tag{50}$$

The peak of the spectrum is given by

$$k_p = \frac{g}{(1.2U_{10})^2}. \tag{51}$$

$S_{in}$ is specified by Hasselmann et al. (1988) in the WAM wave model formulation for wind input energy to waves:

$$S_{in}(k,\theta) = \beta E(k,\theta), \tag{52}$$

where

$$\beta = \max\left[0, 0.25\frac{\rho_a}{\rho_w}\left(28\frac{u_*^a}{C}\cos\theta - 1\right)\right]\omega, \tag{53}$$

in which $u_*^a = \sqrt{C_d}|U_{10}|$ is the air friction velocity, and the phase velocity is given by $C = \omega/k$. The dissipation source function is taken as follows (Hasselmann et al., 1988; Komen et al., 1994):

$$S_{ds}(k,\theta) = -2.25\langle\omega\rangle(\langle k\rangle^2 m_0)^2\left(\frac{k}{\langle k\rangle}+\left(\frac{k}{\langle k\rangle}\right)^2\right)E(k,\theta), \tag{54}$$

where

$$m_0 = \iint E(k,\theta)dk\,d\theta, \tag{55}$$

$$\langle\omega\rangle = \left[m_0^{-1}\iint E(k,\theta)\omega^{-1}dk\,d\theta\right]^{-1}, \tag{56}$$

$$\langle k\rangle = \left[m_0^{-1}\iint E(k,\theta)k^{-1/2}dk\,d\theta\right]^{-2}. \tag{57}$$

Various calculations were done for different wind speeds and different values of $\delta$, and the results show that the agreement between the WKB approximate solution and the exact solution (results of the numerical and the exact solutions are indistinguishable) is excellent if the parameter $\delta$ is small enough. The disparity increases with increase in $\delta$. For example, Fig. 1 shows the approximation solution (47), the exact solutions (A.6) and the numerical solutions from (C.4) for wind speed $U_{10} = 10$ m/s, $\delta = 1/d_e$, $\delta = 2/d_e$ and $\delta = 3/d_e$. Here, $A_v(0) = \kappa u_* z_{0S}$, as Mellor and Blumberg (2004) suggested, $z_{0S}$ is taken as $z_{0S} = 665(1.2/\sqrt{C_d})^{1.5}(u_*^2/g)$, $z$ and velocities ($u_{WE2}$ or $v_{WE2}$) are nondimensionalized, respectively, by $d_e$ and $u_*$, and $d_e = \sqrt{(2A_v(0)/|f|)}$ can be viewed as the depth of the Ekman layer.

### 4.3. Case 3, eddy viscosity decreasing exponentially with depth

Taking $\delta = 0$ in Eq. (27), we have

$$A_v = A_v(0)e^{\alpha z}. \tag{58}$$

The exact solution of Eqs. (1)–(5) for the eddy viscosity (58) is presented by (B.7) in Appendix B. Substituting this form (58) of $A_v$ into Eqs. (18)–(26), we have

$$B(z) = \exp\left(-\frac{\alpha}{4}z\right), \quad D(z) = \frac{2}{\alpha}(1+i)y_0\left(1-\exp\left(-\frac{\alpha}{2}z\right)\right), \tag{59}$$

$$c_1(z) = \frac{1-i}{2\sqrt{2fA_v(0)}}\int_0^z [ifU_s(z')+T_{wds}(z')] \times \exp\left\{-\frac{\alpha}{4}z' - \frac{2}{\alpha}(1+i)y_0\left(1-\exp\left(-\frac{\alpha}{2}z'\right)\right)\right\}dz', \tag{60}$$

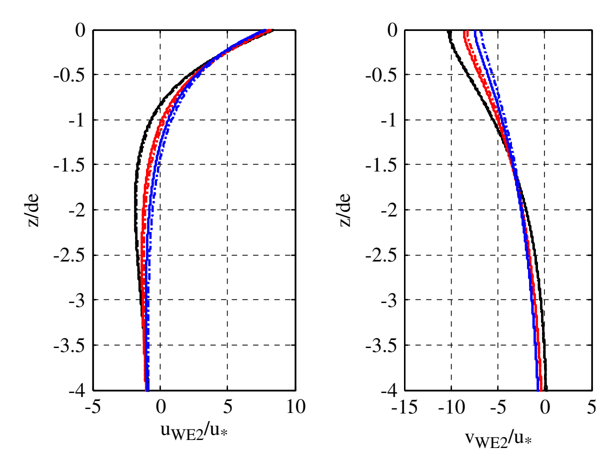


**Fig. 1.** The dimensionless velocities $u_{WE2}/u_*$ (left) and $v_{WE2}/u_*$ (right) calculated from approximation solution (47) (dash-dotted lines), the exact solution (A.6) (solid lines) and the numerical solution (C.4) (dotted lines) for wind speed $U_{10} = 10$ m/s with $\delta = 1/d_e$ (black lines), $\delta = 2/d_e$ (red lines) and $\delta = 3/d_e$ (blue lines). (For interpretation of the references to color in this figure legend, the reader is referred to the web version of this article.)

$$c_2(z) = -\frac{1-i}{2\sqrt{2fA_v(0)}}\int_0^z [ifU_s(z') + T_{wds}(z')] \times \exp\left\{-\frac{\alpha}{4}z' + \frac{2}{\alpha}(1+i)y_0\left(1-\exp\left(-\frac{\alpha}{2}z'\right)\right)\right\}dz', \tag{61}$$

$$\hat{c}_1 = \frac{(\tau_a - \tau_{in})}{A_v(0)\rho_w}\left[-\frac{\alpha}{4} + (1+i)y_0\right]^{-1} - \frac{\alpha + 4(1+i)y_0}{\alpha - 4(1+i)y_0}\hat{c}_2, \tag{62}$$

$$\hat{c}_2 = -\frac{1-i}{2\sqrt{2fA_v(0)}}\int_{-\infty}^0 [ifU_s(z') + T_{wds}(z')] \times \exp\left\{-\frac{\alpha}{4}z' + \frac{2}{\alpha}(1+i)y_0\left(1-\exp\left(-\frac{\alpha}{2}z'\right)\right)\right\}dz', \tag{63}$$

where $y_0 = \sqrt{(f/2A_v(0))}$.

The solution of Eq. (9) reduces to

$$U_{WE3}(z) = [\hat{c}_1 + c_1(z)]\exp\left\{-\frac{\alpha}{4}z + \frac{2}{\alpha}(1+i)y_0\left(1-\exp\left(-\frac{\alpha}{2}z\right)\right)\right\} + [\hat{c}_2 + c_2(z)]\exp\left\{-\frac{\alpha}{4}z - \frac{2}{\alpha}(1+i)y_0\left(1-\exp\left(-\frac{\alpha}{2}z\right)\right)\right\}. \tag{64}$$

As in case 2, the comparisons of the WKB approximate solution (64) with the exact solution (B.7) presented in the Appendix B as well as the numerical solution are made by using the Donelan and Pierson (1987) wavenumber spectrum, the WAM wave model formulation for wind input energy to waves, and wave energy dissipation converted to currents. The results show that the agreement between the WKB approximate solution $u_{WE3}$ and the exact solution (results of the numerical and the exact solutions are indistinguishable) is excellent for any given wind speed if the parameter $\alpha$ is small enough. The disparity increases with increase in $\alpha$. For example, Fig. 2 shows the comparison results for $U_{10}=10$ m/s with $\alpha=0.1/d_e$, $\alpha=0.7/d_e$ and $\alpha=1.2/d_e$.

### 4.4. Case 4, eddy viscosity having a mid-layer peak

If $(\partial A_v(z)/\partial z)=0$ at $z=z_m$ for Eq. (27), then $\alpha=(\delta/1-\delta z_m)$ and Eq. (27) reduces to

$$A_v(z) = A_v(0)(1-\delta z)\exp(\delta z/(1-\delta z_m)). \tag{65}$$

For this case, the eddy viscosity profile has a mid-layer peak at $z=z_m$, it is similar to that shown by O'Brien (1970) or those presented by McWilliams et al. (1997) and Zikanov et al. (2003) using large eddy simulations. This form of eddy viscosity (65) has been used by Tan (2001) in studying atmospheric Ekman boundary layer.

Substituting this form (65) of $A_v$ into Eqs. (18)–(26), we have

$$B(z) = (1-\delta z)^{-1/4}\exp\left(-\frac{\delta}{4(1-\delta z_m)}z\right), \tag{66}$$

$$D(z) = (1+i)\sqrt{\frac{f}{2A_v(0)}}\int_0^z (1-\delta z')^{-1/2}\exp\left(-\frac{\delta}{2(1-\delta z_m)}z'\right)dz'. \tag{67}$$

and the corresponding WKB approximate solution for this case can be calculated by Eqs. (9), (18), (19), (66), (67) and (21)–(26).

Similarly, the comparisons of the WKB approximate solutions with the numerical solution are made for this case of the eddy viscosity. Figs. 3 and 4 show the comparison results for $U_{10}=10$ m/s with different values of $z_m$ and $\delta$. It is also noted that the agreement between the WKB approximate solution and the numerical solution is excellent for a given $U_{10}$ and $z_m$ if the parameter $\delta$ is small enough. The disparity will increase with increase in $\delta$.

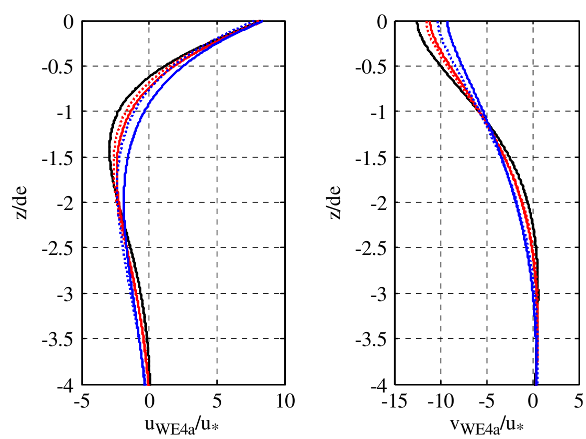


**Fig. 3.** The dimensionless velocities $u_{WE4a}/u_*$ (left) and $v_{WE4a}/u_*$ (right) calculated from the approximate solution (solid lines) and the numerical solution (dotted lines) for wind speed $U_{10}=10$ m/s, $z_m=-20$ m with $\delta=0.1/d_e$ (black lines), $\delta=1/d_e$ (red lines), $\delta=2/d_e$ (blue lines). (For interpretation of the references to color in this figure legend, the reader is referred to the web version of this article.)

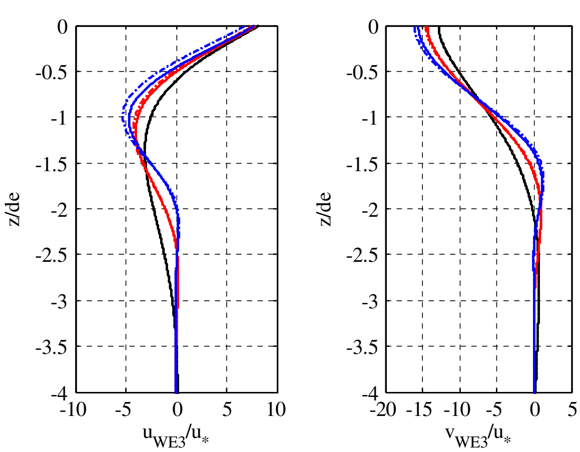


**Fig. 2.** The dimensionless velocities $u_{WE3}/u_*$ (left) and $v_{WE3}/u_*$ (right) calculated from approximation solution (64) (dash-dotted lines), the exact solution (B.7) (solid lines) and the numerical solution (C.4) (dotted lines) for wind speed $U_{10}=10$ m/s with $\alpha=0.1/d_e$ (black lines), $\alpha=0.7/d_e$ (red lines) and $\alpha=1.2/d_e$ (blue lines). (For interpretation of the references to color in this figure legend, the reader is referred to the web version of this article.)

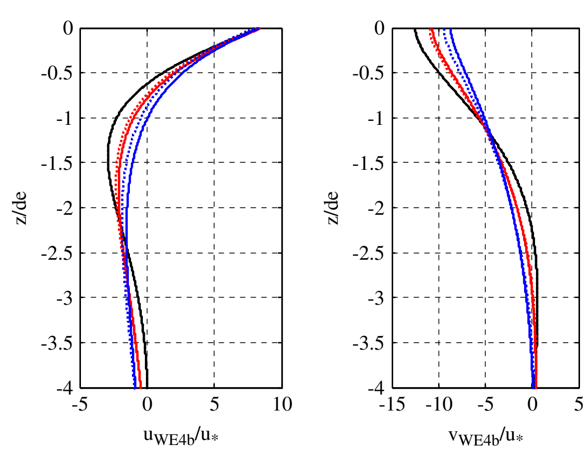


**Fig. 4.** The dimensionless velocities $u_{WE4b}/u_*$ (left) and $v_{WE4b}/u_*$ (right) calculated from the approximate solution (solid lines) and the numerical solution (dotted lines) for wind speed $U_{10}=10$ m/s, $z_m=-50$ m with $\delta=0.1/d_e$ (black lines), $\delta=1/d_e$ (red lines) and $\delta=2/d_e$ (blue lines). (For interpretation of the references to color in this figure legend, the reader is referred to the web version of this article.)

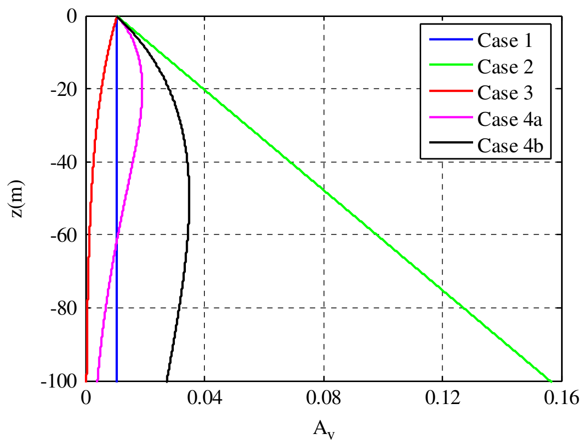


**Fig. 5.** The five kinds of vertical eddy viscosity coefficients $A_v(z)$ for wind speed $U_{10}=10$ m/s: Case 1 with $A_v=\kappa u_* z_{0S}$, Case 2 of Eq. (40) with $\delta=2/d_e$, Case 3 of Eq. (58) with $\alpha=0.5/d_e$, Case 4a of Eq. (65) with $z_m=-20$ m and $\delta=2/d_e$, Case 4b of Eq. (65) with $z_m=-50$ m and $\delta=2/d_e$.

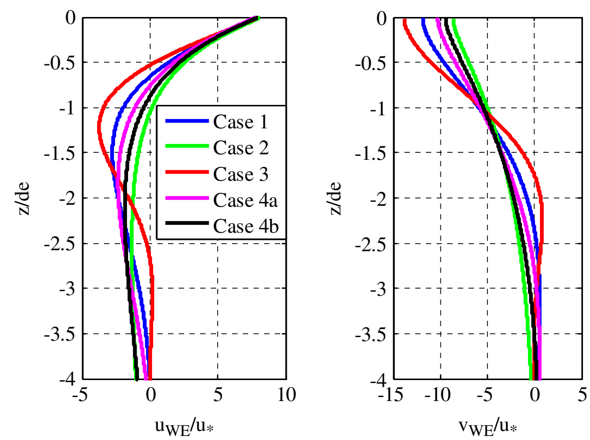


**Fig. 6.** The corresponding dimensionless velocities $u_{WE}/u_*$ (left) and $v_{WE}/u_*$ (right) calculated from the numerical solution (C.4) for the five kinds of vertical eddy viscosity coefficients given by Fig. 5 with wind speed $U_{10}=10$ m/s.

To illustrate the dependence of the solution on the vertical eddy viscosity coefficient $A_v(z)$, Fig. 6 shows the dimensionless velocities $u_{WE}/u_*$ and $v_{WE}/u_*$ calculated from the numerical solution (C.4) for wind speed $U_{10}=10$ m/s with the five kinds of eddy viscosity coefficients given in Fig. 5. It can be noted that the current profiles obviously depend on the form of the vertical eddy viscosity coefficient.

## 5. Conclusions and discussions

An approximate steady solution is obtained using the WKB method with the variation of parameters technique for wave-modified Ekman equations when the eddy viscosity coefficient is gradually varying with depth. The solution presented depends on the two-dimensional wave-number spectrum of ocean waves, wind speed, the Coriolis parameter and the densities of air and water, and it reduces to the exact solution presented by Song (2009) if the eddy viscosity coefficient is taken as a constant. As illustrative examples, we considered a fully developed wind-generated sea with different wind speeds and a kind of gradually varying eddy viscosity. Wave-modified current profiles were calculated and compared with those of the exact solution and numerical solution by using the Donelan and Pierson (1987) wavenumber spectrum, the WAM wave model formulation for wind input energy to waves, and wave energy dissipation converted to currents. A satisfactory agreement between the WKB solution and both the exact solution and the numerical solution were found. The WKB solution that has been derived for the Ekman layer could be employed in theoretical analysis, or for a fast estimation of the Ekman layer profiles in applied research when a near-neutral stratification is encountered. The main conclusion of our research is that: the WKB method is a powerful and elegant singular perturbation method, which can be applied to find an approximate solution of the wave-modified Ekman current. Illustrative examples for a fully developed sea show that the Ekman layer currents are significantly influenced by the surface waves and the vertical variation of the eddy viscosity.

The approximate solution and the method proposed may be more useful in the real ocean when the eddy viscosity was determined by fitting the observational data or the numerical results. Applying the non-dimensional form of the eddy viscosity (27) to fit that obtained by Zikanov et al. (2003) for the flow in the $f$-plane using the numerical method of large-eddy

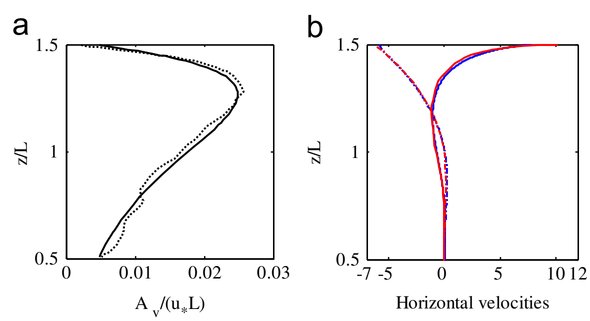


**Fig. 7.** (a) Comparison of the eddy viscosity $\tilde{A}_v(\tilde{z})$ of Eq. (68) (solid line) with that (dotted line) obtained by Zikanov et al. (2003) and (b) comparisons of the horizontal velocities $u/u_*$ and $v/u_*$ calculated by the WKB approximate solution (blue lines) with the corresponding results (red lines) of Zikanov et al. (2003). The horizontal velocities $u/u_*$ and $v/u_*$ are plotted by the solid and dotted lines, respectively. (For interpretation of the references to color in this figure legend, the reader is referred to the web version of this article.)

simulations (LES) gives

$$\tilde{A}_v(\tilde{z})=0.004[1-64.0327(\tilde{z}-1.5)]\exp[4.0073(\tilde{z}-1.5)], \quad (68)$$

here, both the Cartesian coordinate system and the scales used in the dimensionless form are taken the same as those of Zikanov et al. (2003), the fitting method is the least square fit. $\tilde{A}_v(\tilde{z})=A_v(z)/(u_* L)$, $\tilde{z}=z/L$, $L=u_*/|f|$ is used as the length scale, and the surface friction velocity $u_*$ is taken as the velocity scale. Fig. 7(a) shows the comparison of the eddy viscosity (68) (solid line) with that (dotted line) obtained by Zikanov et al. (2003) using LES. The mean current profiles (red lines) of Zikanov et al. (2003) are compared with the WKB approximate solution (blue lines) in Fig. 7(b). Here and below, the approximate solutions are calculated as in the Section 4 by assuming a fully developed sea. The comparisons of Fig. 7(b) show that both $u/u_*$ (solid lines) and $v/u_*$ (dotted lines) calculated by the two methods are the quite consistent.

Using the Cartesian coordinate system as stated in Section 2, the dimensional $A_v(z)$ corresponding to Eq. (68) can be written as

$$A_v(z)=0.004u_*^2(1-64.0327z|f|/u_*)\exp\{4.0073z|f|/u_*\}/|f|. \quad (69)$$

The horizontal velocities $u$ and $v$ predicted by the WKB approximate solution (solid lines) using the eddy viscosities (69) with $u_*$ and $f$ corresponding to the observations of LOTUS and EBC (Price and Sundermeyer, 1999) are shown in Fig. 8 to compare with the observation results (stars). The classical Ekman solutions (dotted

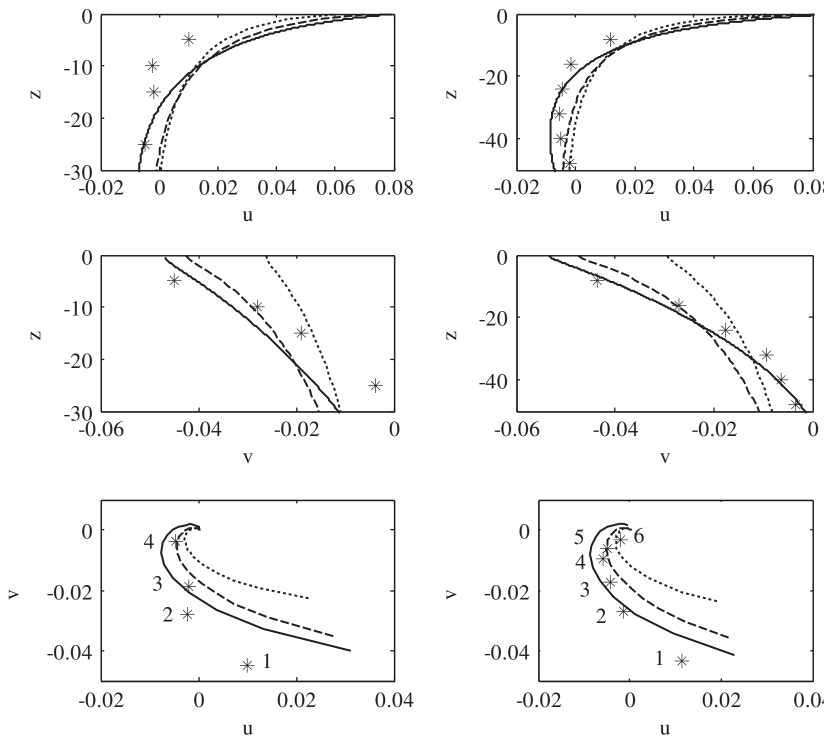


**Fig. 8.** Comparison of the WKB approximate solutions with the LOTUS3 (left) and EBC (right) data, denoted with star. The depths of the experimental data points are marked by the numbers. The numbers from 1 to 4 appeared on the left panel subfigures are, respectively, corresponding to the depths of $z=-5$, $-10$, $-15$ and $-25$ m, and the numbers from 1 to 6 appeared on the right panel subfigures are, respectively, corresponding to the depths of $z=-8$, $-16$, $-24$, $-32$, $-40$ and $-48$ m. The solid lines are the WKB approximate solutions with the eddy viscosity having a mid-layer peak. The dotted lines are the classical Ekman solutions and the dashed lines are the solutions presented by Song (2009) for the eddy viscosity varies linearly with depth. The top panel depicts the downwind velocities as functions of depth, and the middle panel shows the crosswind, respectively. The bottom panels depict hodograms that display the downwind velocity plotted against the crosswind velocity.

lines) and the solutions (dashed lines) presented by Song (2009) for eddy viscosity varies linearly with depth are also shown in Fig. 8. For the LOTUS3 comparison, the solution is obtained by using $U_{10}=6.8$ m/s, $f=8.36\times10^{-5}\,\mathrm{s}^{-1}$ and $A_v(z)=0.0032(1-0.6528z)\exp(0.0409z)$. For the EBC comparison, $U_{10}=7.6$ m/s, $f=8.77\times10^{-5}\,\mathrm{s}^{-1}$ and $A_v(z)=0.004(1-0.6003z)\exp(0.0376z)$ are used. The profiles of Fig. 8 show that there are considerable deviations from the classical Ekman profiles, which Price and Sundermeyer (1999) attribute to dynamical effects of mixed layer stratification and diurnal variations in the mixed layer depth. However, the comparisons between observations and the theoretical predictions as shown in Fig. 8, demonstrate that both the preferred eddy viscosity and the inclusion of the Stokes drift, wind input and wave dissipation can largely reduce these discrepancies.

A complex eddy viscosity possibly can be inferred from the ratio of the observed turbulent stress and shear due to the nonparallel shear–stress relation, which may be result from the time averaging over the cycling of the stratification in response to diurnal buoyancy fluxes (Price and Sundermeyer, 1999; Lenn and Chereskin, 2009). It should be noted that the WKB approximate solution and the method proposed are still valid for such complex eddy viscosity. Taking the form of Eq. (27) as the complex eddy viscosity to fit (the least square fit) that presented by Lenn and Chereskin (2009) gives

$$A_v(z)=(0.0222-0.0534i)[1-(0.1757+0.1795i)z]\times\exp[(0.0509+0.0084i)z] \qquad (70)$$

Fig. 9(a) shows the comparison of the eddy viscosity (70) with that presented by Lenn and Chereskin (2009). Fig. 9(b) shows the comparisons of the horizontal velocities $u$ and $v$ calculated by the WKB approximate solution with the corresponding results of Lenn and Chereskin (2009). The approximate solution is

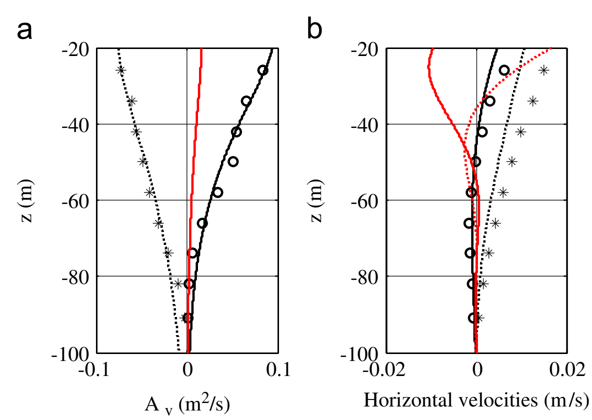


**Fig. 9.** (a) Real (circles) and imaginary (stars) components of the inferred eddy viscosity $A_v(z)$ by Lenn and Chereskin (2009) and a least squares fit of it (solid and dotted black lines). Solid red line shows the eddy viscosity (69) corresponding to $u_*=0.0091$ and $f=-1.2612\times10^{-4}$ extracted from the observations of Lenn and Chereskin (2009). (b) the comparisons of the horizontal velocities $u$ and $v$ calculated by the WKB approximate solution (solid line for $u$, dotted line for $v$) with the observation (circles for $u$, stars for $v$) of Lenn and Chereskin (2009). Here, the horizontal velocities corresponding to Eqs. (69) and (70) are plotted by red and black lines, respectively. (For interpretation of the references to color in this figure legend, the reader is referred to the web version of this article.)

calculated using the wind stress presented by Lenn and Chereskin (2009) from the wind product of blended QuickSCAT and NCEP reanalysis winds. The comparisons of Fig. 9(b) show that both $u$ and $v$ calculated by the WKB approximate solution using the eddy viscosity (70) are quite in agreement with the observation of Lenn and Chereskin (2009). To compare the current profiles obtained using the complex eddy viscosity proposed by

Lenn and Chereskin (2009) with those estimated by the real one such as Eq. (69), we also include the WKB approximate solutions obtained using the eddy viscosity (69) with $u_*=0.0091$ m/s and $f=-1.2612\times10^{-4}\,\mathrm{s}^{-1}$ extracted from the observations of Lenn and Chereskin (2009) in Fig. 9(b). The current profiles obtained using the eddy viscosity (69) of Fig. 9(b) show that there are considerable deviations from those observed by Lenn and Chereskin (2009), which may be caused by the great difference between the eddy viscosity (69) and that presented by Lenn and Chereskin (2009) as shown in Fig. 9(a).

It is noted that the corresponding solutions can be obtained by using the wave spectrum from the wave model for a more general developing sea, although we only illustrate the current profiles for a fully developed wind-generated sea as examples. Furthermore, the steady solutions presented in the paper may be extended to the time-dependent cases using a Laplace transform technique analogous to that of Lewis and Belcher (2004) in the study of the effects of the Stokes drift on Ekman current. It is also noted that we neglected many other contributions to Ekman surface currents, for example, density stratification, surface heating, buoyancy flux and the horizontal component of the Coriolis frequency. These effects can be important in certain situations and should be considered for accurate modeling of surface currents, but are also beyond the scope of the present study. Especially, as Price, Sundermeyer (1999) and Rascle (2007) demonstrated, variable surface buoyancy fluxes and near-surface stratification have a significant impact on the Ekman layer. It is therefore of obvious importance to extend the present study to the stratified condition. Furthermore, the parameterization forms of wave-current interactions involving $S_{in}$ and $S_{ds}$ also affected the presented solutions, which needs further investigated.

## Appendix A. Exact solutions for eddy viscosity increasing linearly with depth

Substituting eddy viscosity (40) into Eqs. (1) and (2), we have

$$\left(z_+ + \frac{1}{\delta}\right)\frac{\partial^2 U_{WE2}(-z_+)}{\partial z_+^2} + \frac{\partial U_{WE2}(-z_+)}{\partial z_+} - \frac{if}{A_v(0)\delta}U_{WE2}(-z_+) = \frac{[ifU_s(-z_+)+T_{wds}(-z_+)]}{A_v(0)\delta}, \tag{A.1}$$

$$\left(z_+ + \frac{1}{\delta}\right)\frac{\partial U_{WE2}(-z_+)}{\partial z_+} = -\frac{(\tau_a-\tau_{in})}{\rho_w \kappa u_*},\quad z_+=0, \tag{A.2}$$

where $U_{WE2}$ is the modified complex horizontal velocity corresponding to eddy viscosity (40).

The general solution of (A.1) is

$$U_{WE2}(-z_+) = B_1 I_0(\eta) + B_2 K_0(\eta) + \Psi_0(-z_+), \tag{A.3}$$

where $B_1$ and $B_2$ are constants to be determined, $\eta=(2/\delta)\sqrt{(if(1+\delta z_+)/A_v(0))}$, $I_0$ and $K_0$ are the first and the second kinds of modified Bessel functions, respectively, and $\Psi_0(-z_+)$ is a special solution of (A.1) as follows:

$$\Psi_0(-z_+) = -\frac{2}{A_v(0)\delta}\left\{I_0(\eta)\int_{z_+}^{+\infty} K_0(\eta')[ifU_s(-z')+T_{wds}(-z')]dz' - K_0(\eta)\int_{z_+}^{+\infty} I_0(\eta')[ifU_s(-z')+T_{wds}(-z')]dz'\right\}, \tag{A.4}$$

where $\eta' = \frac{2}{\delta}\sqrt{(if(1+\delta z')/A_v(0))}$.

The boundary condition $U_{WE2}\to 0$ as $z_+\to+\infty \Rightarrow;\ B_1=0$, whilst the surface condition (5) reduces

$$B_2 = -\frac{2(\tau_a-\tau_{in})}{\rho_w A_v(0)\delta\eta_0 K_0'(\eta_0)} + \frac{2}{A_v(0)\delta} \times\left\{\frac{I_0'(\eta_0)}{K_0'(\eta_0)}\int_0^{+\infty} K_0(\eta')\left[ifU_s(-z')+T_{wds}(-z')\right]dz' - \int_0^{+\infty} I_0(\eta')[ifU_s(-z')+T_{wds}(-z')]dz'\right\}, \tag{A.5}$$

where $\eta_0=(2/\delta)\sqrt{(if/A_v(0))}$, $I_0'$ and $K_0'$, respectively, are the derivatives of $I_0$ and $K_0$.

Thus, the wave-modified Ekman solution of (A.3) is

$$U_{WE2}(-z_+) = -\frac{2(\tau_a-\tau_{in})}{\rho_w A_v(0)\delta\eta_0 K_0'(\eta_0)}K_0(\eta) + \frac{2}{A_v(0)\delta} \times\left\{\frac{I_0'(\eta_0)}{K_0'(\eta_0)}K_0(\eta)\int_0^{+\infty} K_0(\eta')\left[ifU_s(-z')+T_{wds}(-z')\right]dz' - K_0(\eta)\int_0^{z_+} I_0(\eta')[ifU_s(-z')+T_{wds}(-z')]dz' - I_0(\eta)\int_{z_+}^{+\infty} K_0(\eta')[ifU_s(-z')+T_{wds}(-z')]dz'\right\}. \tag{A.6}$$

## Appendix B. Exact solutions for eddy viscosity decreasing exponentially with depth

For eddy viscosity (58), the general solution of Eq. (1) is

$$U_{WE3}(z) = A_1\xi I_1(i^{1/2}\xi) + A_2\xi K_1(i^{1/2}\xi) + \Psi_1(z), \tag{B.1}$$

where $\xi=(2/\alpha)\sqrt{(f/A_v(0))}e^{-\alpha z/2}$, $A_1$ and $A_2$ are constants to be determined, $I_1$ and $K_1$ are the first and the second kinds of modified Bessel functions of order one, respectively, and $\Psi_1(z)$ is a special solution of Eq. (1) as follows:

$$\Psi_1(z) = C_1(z)\xi I_1(i^{1/2}\xi) + C_2(z)\xi K_1(i^{1/2}\xi), \tag{B.2}$$

where

$$C_1(z) = -\frac{\alpha}{2f}\int_0^z \xi' K_1(i^{1/2}\xi')\left[ifU_s(z')+T_{wds}(z')\right]dz', \tag{B.3}$$

$$C_2(z) = \frac{\alpha}{2f}\int_0^z \xi' I_1(i^{1/2}\xi')\left[ifU_s(z')+T_{wds}(z')\right]dz', \tag{B.4}$$

with $\xi'=(2/\alpha)\sqrt{(f/A_v(0))}e^{-\alpha z'/2}$.

Using the boundary condition $U_{WE3}\to 0$ as $z\to-\infty$, we have

$$A_1 = -C_1(-\infty) = -\frac{\alpha}{2f}\int_{-\infty}^0 \xi' K_1(i^{1/2}\xi')\left[ifU_s(z')+T_{wds}(z')\right]dz', \tag{B.5}$$

whilst the surface condition (2) reduces

$$A_2 = \frac{I_0(\xi_0)}{K_0(\xi_0)}A_1 + \frac{\alpha(\tau_a-\tau_{in})}{2\rho_w i^{1/2} f K_0(\xi_0)}, \tag{B.6}$$

where $\xi_0=i^{1/2}(2/\alpha)\sqrt{(f/A_v(0))}$, $I_0$ and $K_0$, respectively, are the first and the second kinds of modified Bessel functions of zero order. Thus, the exact solution of Eqs. (1)–(5) for eddy viscosity (58) is

$$U_{WE3}(z) = [A_1 + C_1(z)]\xi I_1(i^{1/2}\xi) + \left[\frac{I_0(\xi_0)}{K_0(\xi_0)}A_1 + \frac{\alpha(\tau_a-\tau_{in})}{2\rho_w i^{1/2} f K_0(\xi_0)} + C_2(z)\right]\xi K_1(i^{1/2}\xi), \tag{B.7}$$

where $A_1$, $C_1(z)$ and $C_2(z)$ are, respectively, presented by (B.5), (B.3) and (B.4).

## Appendix C. Numerical solutions for Eqs. (1)–(5)

The discretization form of Eq. (1) is as follows:

$$\left(\frac{A_v^i}{\Delta z^2} + \frac{A_v'^i}{\Delta z^2}\right)U_{WE}^{i-1} + \left(\frac{-2A_v^i - A_v'^i}{\Delta z^2} - if\right)U_{WE}^i + \frac{A_v^i}{\Delta z^2}U_{WE}^{i+1} = ifU_s^i + T_{wds}^i, \tag{C.1}$$

where superscript $i$ represents the depth of $z_i$, $\Delta z=0.01$ m.

The discretization form for the surface boundary condition is

$$\frac{A_v(0)}{\Delta z}U_{WE}^1-\frac{A_v(0)}{\Delta z}U_{WE}^2=\frac{\tau_a-\tau_{in}}{\rho_w},(z_1=0), \tag{C.2}$$

and the corresponding discretization of the lower boundary condition is taken as

$$U_{WE}^n=0,(z_n=-1500\,\text{m}) \tag{C.3}$$

Then we can have

$$\begin{bmatrix} B_1 & C_1 & & & & \\ A_2 & B_2 & C_2 & & & \\ & A_i & B_i & C_i & & \\ & & A_{n-1} & B_{n-1} & C_{n-1} \\ & & & A_n & B_n \end{bmatrix}\cdot\begin{bmatrix} U_{WE}^1 \\ U_{WE}^2 \\ U_{WE}^i \\ U_{WE}^{n-1} \\ U_{WE}^n \end{bmatrix}=\begin{bmatrix} D_1 \\ D_2 \\ D_i \\ D_{n-1} \\ D_n \end{bmatrix} \tag{C.4}$$

where $B_1=(A_v(0)/\Delta z)$,$C_1=-(A_v(0)/\Delta z)$,$D_1=(\tau_a-\tau_{in}/\rho_w)$, $A_n=0$, $B_n=1$, $D_n=0$; $A_i=(A_v^i/\Delta z^2)+(A_v'^i/\Delta z^2)$, $B_i=(-2A_v^i-A_v'^i/\Delta z^2)-if$, $C_i=(A_v^i/\ \Delta z^2)$, $D_i=ifU_s^i+T_{wds}^i(i=2,3,\ \ldots,n-1)$. We can use the matrix chase-after method to solve Eq. (C.4).

## References


Andreas, E.L., Emanuel, K.A., 2001. Effects of sea spray on tropical cyclone intensity. J. Atmos. Sci. 58, 3741–3751.

Berger, B.W., Grisogono, B., 1998. The baroclinic, variable eddy viscosity Ekman layer: an approximate analytical solution. Boundary–Layer Meteorol. 87, 363–380.

Brickman, D., Frank, K.T., 2000. Modelling the dispersal and mortality of Browns Bank egg and larval haddock (*Melanogrammus aeglefinus*). Can. J. Fish. Aquat. Sci. 57, 2519–2535.

Chapron, B., Collard, F., Ardhuin, F., 2005. Direct measurements of ocean surface velocity from space: interpretation and validation. J. Geophys. Res. 110, C07008. doi:10.1029/2004JC002809.

Donelan, M.A., Pierson, W.J.P., 1987. Radar scattering and equilibrium ranges in wind-generated waves with application to scatterometry. J. Geophys. Res. 92, 4971–5029.

Emanuel, K.A., 1999. Thermodynamic control of hurricane intensity. Nature 401, 665–669.

Farmer, D.M., D'Asaro, E.A., Trevorrow, M.V., Dairiki, G.T., 1995. Three-dimensional structure in a tidal convergence front. Cont. Shelf Res. 15, 1649–1673.

Grisogono, B., 1995. A generalized Ekman layer profile with gradually varying eddy diffusivities. Q. J. R. Meteorol. Soc. 121, 445–453.

Hasselmann, S., Hasselmann, K., Komen, G.K., Janssen, P., Ewing, J.A., Cardone, V., 1988. The WAM model—a third generation ocean wave prediction model. J. Phys. Oceanogr. 18, 1775–1810.

Huang, N.E., 1971. Derivation of Stokes drift for a deep-water random gravity wave field. Deep-Sea Res. 18, 255–259.

Huang, N.E., 1979. On surface drift currents in the ocean. J. Fluid Mech. 91, 191–208.

Jenkins, A.D., 1986. A theory for steady and variable wind and wave induced currents. J. Phys. Oceanogr. 16, 1370–1377.

Jenkins, A.D., 1987a. A Lagrangian model for wind- and wave-induced near surface currents. Coastal Eng. 11, 513–526.

Jenkins, A.D., 1987b. Wind and wave induced currents in a rotating sea with depth varying eddy viscosity. J. Phys. Oceanogr. 17, 938–951.

Jenkins, A.D., 1989. The use of a wave prediction model for driving a near surface current model. Dtsch. Hydrogr. Z. 42, 134–149.

Kelly, K.A., Dickinson, S., McPhaden, M., Johnson, G.C., 2001. Ocean currents evident in satellite wind data. Geophys. Res. Lett. 28, 2469–2472.

Kenyon, K.E., 1969. Stokes drift for random gravity waves. J. Geophys. Res 74, 6991–6994.

Komen, G.J., Cavaleri, L., Donelan, M., Hasselmann, K., Hasselmann, S., Janssen, P.A.E.M., 1994. Dynamics and Modelling of Ocean Waves. Cambridge University Press, Cambridge.

Leibovich, S., 1997a. Surface and near-surface motion of oil in the sea: part I. Final Rep. to US. Minerals Management Service, Contract 14-35-0001-30612, 136.

Leibovich, S., 1997b. Surface and near-surface motion of oil in the sea: part II. Final Rep. to US. Minerals Management Service, Contract 14-35-0001-30612, 24 pp.

Lenn, Y.D., Chereskin, T.K., 2009. Observation of Ekman currents in the southern ocean. J. Phys. Oceanogr. 39, 768–779.

Lewis, D.M., Belcher, S.E., 2004. Time-dependent, coupled, Ekman boundary layer solutions incorporating Stokes drift. Dyn. Atmos. Oceans 37, 313–351.

Madsen, O.S., 1977. A realistic model of the wind-induced Ekman boundary layer. J. Phys. Oceanogr. 7, 248–255.

McWilliams, J.C., Sullivan, P.P., Moeng, C.H., 1997. Langmuir turbulence in the ocean. J. Fluid Mech. 334, 1–30.

Mellor, G., Blumberg, A., 2004. Wave breaking and ocean surface layer thermal response. J. Phys. Oceanogr. 34, 693–698.

Melsom, A., 1996. Effects of wave breaking on the surface drift. J. Geophys. Res. 101 (C5), 12071–12078.

Morinta, I., Sugioka, S., Kojima, T., 1997. Real-time forecasting model of oil spill spreading. In: Proceedings of the 1997 International Oil Spill Conference, Washington, DC, American Petroleum Institute, pp. 559–566.

O'Brien, J.J., 1970. A note on the vertical structure of the eddy exchange coefficient in the planetary boundary layer. J. Atmos. Sci. 27, 1213–1215.

Perrie, W., Tang, C., Hu, Y., DeTracy, B.M., 2003. The impact of waves on surface currents. J. Phys. Oceanogr. 33, 2126–2140.

Polton, J.A., Lewis, D.M., Belcher, S.E., 2005. The role of wave-induced Coriolis–Stokes forcing on the wind-driven mixed layer. J. Phys. Oceanogr. 35, 444–457.

Price, J., Sundermeyer, M.A., 1999. Stratified Ekman layers. J. Geophys. Res. 104, 20467–20494.

Quilfen, Y., Chapron, B., Vandemark, D., 2001. The ERS scatterometer wind measurement accuracy: Evidence of seasonal and regional biases. J. Atmos. Oceanic Technol. 18 (10), 1684–1697.

Rascle, N., Ardhuin, F., Terray, E.A., 2006. Drift and mixing under the ocean surface: a coherent one-dimensional description with application to unstratified conditions. J. Geophys. Res. 111, C03016. doi:10.1029/2005JC003004.

Rascle, N., 2007. Wave Effects on the Ocean Circulation. Ph.D. Thesis, Universite de Bretagne Occidentale, 〈http://tel.archives-ouvertes.fr/tel-00182250/en〉.

Reiss, C., Panteleev, G., Taggart, C., Sheng, J., de Young, B., 2000. Observations on larval fish transport and retention on the Scotian Shelf in relation to geostrophic circulation. Fish. Oceanogr. 9, 195–213.

Santiago-Mandujano, F., Firing, E., 1990. Mixed-layer shear generated by wind stress in the central equatorial Pacific. J. Phys. Oceanogr. 20, 1576–1582.

Song, J.B., 2009. The effects of random surface waves on the steady Ekman current solutions. Deep-Sea Res. Part I 56 (5), 659–671.

Tan, Z.M., 2001. An approximate analytical solution for the baroclinic and variable eddy diffusivity semi-geostrophic Ekman boundary layer. Boundary–Layer Meteorol. 98, 361–385.

Tang, C.L., Gui, Q., 1996. A dynamical model for wind-driven ice motion: application to ice drift on the Labrador Shelf. J. Geophys. Res. 101, 28343–28364.

Tang, C.L., McFarlane, N.A., D'Alessio, S.J.D., 2002. Boundary layer models for the ocean and atmosphere. In: Perrie, W. (Ed.), Atmosphere–Ocean Interactions. WIT Press, pp. 223–264.

Tang, C.L., Perrie, W., Jenkins, A.D., DeTraccy, B.M., Hu, Y., Toulany, B., 2007. Observation and modeling of surface currents on the Grand Banks: a study of the wave effects on surface currents. J. Geophys. Res. 112, C10025. doi:10.1029/2006JC004028.

Weber, J.E., 1983. Steady wind- and wave-induced currents in the open ocean. J. Phys. Oceanogr. 13, 524–530.

Weber, J.E., Melsom, A., 1993. Transient ocean currents induced by wind and growing waves. J. Phys. Oceanogr. 23, 193–206.

Witten, A.J., Thomas, J.H., 1976. Steady wind-driven currents in a large lake with depth-dependent eddy viscosity. J. Phys. Oceanogr. 6, 85–92.

Wu, J., 1982. Wind-stress coefficients over sea surface from breeze to hurricane. J. Geophys. Res. 87 (C12), 9704–9706.

Zikanov, O., Slinn, D.N., Dhanak, M.R., 2003. Large-eddy simulations of the wind-induced turbulent Ekman layer. J. Fluid Mech. 495, 343–368.